

Doxorubicin-induced oxidative stress and endothelial dysfunction in conduit arteries is prevented by mitochondrial-specific antioxidant treatment

Zachary S. Clayton, PhD¹, Vienna E. Brunt, PhD¹, David A. Hutton, BA¹, Nicholas S. VanDongen, MS¹, Angelo D'Alessandro, PhD², Julie A. Reisz, PhD², Brian P. Ziemba, PhD¹ & Douglas R. Seals, PhD^{1,2}

¹Department of Integrative Physiology, University of Colorado Boulder, Boulder, CO, USA

²Department of Medicine, Anschutz Medical Campus, University of Colorado Denver, Aurora, CO, USA

Supplemental Materials

Supplemental Materials and Methods

Animals

Male C57BL6/J mice were purchased from Jackson Laboratories at 3 months of age and allowed to acclimate to our facilities for 4 weeks prior to beginning the study. Mice were housed in standard cages on a 12:12 h light:dark cycle and body mass, energy intake and water consumption were monitored throughout the study. All mice were allowed access to normal rodent chow (Harlan 7917) and water *ad libitum*. Mice were randomly assigned to receive Doxorubicin (DOXO; 10 mg/kg intraperitoneal injection from a 2 mg/ml stock; R & Systems 2252/50 Minneapolis, MN; suspended in sterile 1x PBS) or Sham (intraperitoneal injection of 150 μ L sterile 1x PBS). DOXO and Sham were prepared fresh prior to injection. An additional cohort of mice (n = 5) was supplemented *in vivo* with the mitochondrial-targeted antioxidant MitoQ (250 μ M in the drinking water) as previously described by our laboratory¹, immediately following DOXO administration. Bottles of MitoQ-enriched drinking water were protected from light using foil covering.

Vascular endothelial function.

Four weeks following injection of DOXO or sham, mice were anaesthetized with inhaled isoflurane and sacrificed by exsanguination via cardiac puncture. Endothelium-dependent dilation (EDD) and endothelium-independent dilation were measured in isolated carotid arteries as previously described (1-3). The carotid arteries were dissected free of surrounding tissue and cannulated onto glass micropipettes in warmed (37°C) physiological saline solution in pressure myograph chambers (Danish Myo Technology A/S, Aarhus, Denmark). Arteries were pressurized to 50 mmHg intraluminal pressure and allowed to equilibrate for 45 min prior to the beginning of experiments, as previously described by our laboratory (4,5). Following pre-constriction with phenylephrine (2 μ M; Sigma-Aldrich Corp., St Louis, MO, USA), EDD was assessed by measuring the increase in luminal diameter in response to increasing concentrations of acetylcholine (ACh; 1×10^{-9} Mol/L to 1×10^{-4} Mol/L; Sigma-Aldrich Corp.). Endothelium-independent dilation as measured as dilation in response to increasing doses of the exogenous nitric oxide (NO) donor sodium nitroprusside (SNP; 1×10^{-10} Mol/L to 1×10^{-4} Mol/L; Sigma-Aldrich Corp). Following all dose responses, maximal carotid artery diameter was confirmed by 20-30 min incubation in Ca^{2+} -free physiological saline solution. To account for baseline differences in vessel diameter, all dose-response data are reported on a percentage basis.

NO-mediated EDD.

EDD was assessed in the presence of the endothelial NO synthase inhibitor N^G-nitro-L-arginine methyl ester (L-NAME; 0.1 mMol/L, 30 min incubation; Sigma-Aldrich Corp.), and the contribution of NO (NO-mediated dilation) was calculated as the difference between peak dilation to ACh alone and peak dilation in the presence of L-NAME, as previously described (2).

Tonic ROS suppression of EDD.

Carotid arteries were incubated for 60 min with 1 mMol/L 4-hydroxy-2,2,6,6-tetramethylpiperidin-1-oxyl (TEMPOL), a superoxide dismutase (SOD) mimetic, to scavenge ROS prior to assessment of EDD to ACh (6). Tonic suppression was determined as the increase in peak EDD from ACh alone.

Tonic mitochondrial ROS suppression of EDD.

Carotid arteries were incubated for 60 min with 1 μ Mol/L mitoquinol mesylate (MitoQ) to scavenge mitochondrial ROS prior to assessment of EDD to ACh (1,7).

Aortic whole-cell and mitochondria-specific ROS.

Measurement of ROS in the thoracic aorta was performed using electron paramagnetic resonance (EPR) spectroscopy as previously described (1,2,6,7). Briefly, the aorta was removed and dissected free of surrounding tissue. Segments of 1 mm were incubated for 1 h at 37°C in Krebs-HEPES buffer with the superoxide-specific spin probe 1-hydroxy-3methylcarbonyl-2,2,5,5-tetramethylpyrrolidine (1.0 mMol/L; Enzo Life Sciences, Inc., Farmington, NY, USA) or mitochondrial ROS-specific spin probe MitoTEMPO-H (0.5 mMol/L; Enzo Life Sciences, Inc.) for detection of whole-cell and mitochondria-specific ROS, respectively. The signal amplitude was analyzed using a MS300 X-band EPR spectrometer (Magnettech GmbH, Berlin, Germany) with the following settings: centerfield, 3350 G; sweep, 80 G; microwave modulation, 3000 mG, and microwave attenuation, 7 dB.

Aortic protein abundance.

Protein abundance was measured in segments of thoracic aorta following mechanical homogenization in radio-immunoprecipitation assay lysis buffer supplemented with protease and phosphatase inhibitors (1 mMol/L sodium orthovanadate, 1X complete mini protease inhibitor cocktail tablet [Roche, Mannheim, Germany], 1 mMol/L phenylmethylsulfonyl fluoride, 1:100 Phosphatase Inhibitor Cocktail [Sigma], 5 mMol/L sodium fluoride and 5 mMol/L sodium pyrophosphate). Aortic total protein content was

quantified using a bicinchoninic acid assay (Thermo Fisher Scientific, Eugene, OR). Next, protein abundance of SOD1 (anti-goat; 1:500; R&D Systems, Minneapolis, MN, cat no. AF3787), SOD2 (anti-goat; 1:50; R&D Systems, cat no. AF3419) and SOD3 (anti-rabbit; 1:200; R&D Systems, cat no. MAB34201) were determined by loading 20 ng/mL of aortic protein per capillary in a 25-lane (capillary) automated western blot quantitative analyzer (ProteinSimple, San Jose, California), according to the manufacturer's guidelines, as previously described (3). Anti-goat and anti-rabbit secondary antibodies were provided by the manufacturer and used according to the manufacturer's guidelines. A grayscale analysis of the band intensities to quantify protein abundance was then performed using Compass software (ProteinSimple), with target proteins expressed relative to loading control (GAPDH; 1:200; Cell Signaling, cat no. 2118).

Plasma exposure and ROS cell culture experiments.

Human umbilical vein endothelial cells (HUVECs; Lonza, Basel, Switzerland) were cultured and passaged (10 passages maximum [a passage number in which endothelial cells maintain their phenotype⁸]) at 37°C and 5% CO₂ to ~80% confluency in Endothelial Cell Growth Media (EGM)-2 media (Lonza) supplemented with an additional 2% fetal calf serum (FCS; Sigma-Aldrich Corp.), 100 µg/mL penicillin and 172 µg/mL streptomycin (Gibco, Gaithersburg, MD). Cells were washed with Hanks' balanced salt solution (HBSS), lifted with Trypsin-Like Enzyme (TrypLE) cell dissociation enzyme (Gibco), washed and resuspended in HBSS, counted and diluted to 9 x 10³ cells/mL (designed to result in 60-80% confluency over 48-hour incubation) in FCS-supplemented EGM-2. 100 µL of HUVEC cell suspension was added to each well of a high content image plate with 0.2 mm glass bottom (Corning, Kennebunk, ME) coated with bovine gelatin substrate (Attachment Factor Solution; Cell Applications, Inc., San Diego, CA) to facilitate cell adhesion. After a 24-hour incubation, attached cells were washed once with HBSS and incubated in FCS-free EGM-2 media supplemented with 10% mouse

plasma for 24 hours (37°C, 5% CO₂). Attached cells were then washed twice with HBSS and incubated for the designated amount of time (37°C, 5% CO₂) with a fluorescent probe mixture ([2.9 μMol/L Hoechst 33342 nuclear probe, 9.2 μMol/L CellROX Deep Red ROS probe, 60 minute incubation]; or [2.9 μMol/L Hoechst 33342 nuclear probe, 5 μMol/L MitoSOX Deep Red mitochondrial ROS probe, 10 minute incubation]; or [2.9 μMol/L Hoechst 33342 nuclear probe, 0.2 μMol/L Mito Tracker Green mitochondrial volume probe, 45 minute incubation]). After dye removal and three washes with HBSS, cells were left in 100 μL of HBSS for subsequent imaging. Microscopy was carried out on an EVOS FL microscope (Invitrogen, Carlsbad, CA) set at 20X magnification. Cells were selected for imaging based on characteristic endothelial cell and nuclear morphology. Cell images of CellROX, MitoSOX and Mito Tracker fluorescent dyes were analyzed with Fiji, the open-source processing program distribution of ImageJ (National Institutes of Health) (⁹). For CellROX, MitoSOX and Mito Tracker, image intensity was averaged over the entire cell area.

Supplemental VEGF-A experiments.

HUVEC cells were cultured and passaged in conditions identical to those used for mouse plasma supplementation experiments. Recombinant mouse VEGF 164 (VEGF-A) protein (R&D, Minneapolis, MN, cat no. 493-MV-005) reconstituted in 0.1% w/v bovine serum albumin (BSA) in PBS was mixed with mouse plasma from DOXO-treated mouse plasma and added to FCS-free EGM-2 media for a final concentration of 90 pg/mL VEGF-A and 10% plasma. For control mouse plasma, a similar volume of 0.1% w/v BSA in PBS was mixed with mouse plasma and added to FCS-free EGM-2 media to achieve identical concentrations of plasma, media and vehicle. Both VEGF-A-supplemented mouse plasma derived from DOXO treated mice media solutions and Sham mouse media solutions were added to each well of 60-80% confluent HUVEC cells as in non-VEGF-A supplemented conditions. Fluorescent

probe concentrations were identical, and washes, imaging and analysis were performed identically to this description above.

Plasma metabolomics analysis.

Sample Preparation & UHPLC-MS – hydrophilic metabolite analysis. Prior to LC-MS analysis, samples were placed on ice, and 20 μ L aliquots were diluted with 480 μ L of ice-cold methanol/acetonitrile/water (5/3/2). Extractions were performed and resulting samples analyzed using a 5 min C18 gradient on a Thermo Vanquish-Q Exactive system (San Jose, CA, USA), as previously described (¹⁰).

Sample Preparation – lipid analysis. Prior to LC-MS analysis, samples were placed on Ice, and 10 μ L aliquots were diluted with 90 μ L of ice-cold methanol. Suspensions were vortexed to mix and placed at -20°C for 30 min. Insoluble material was removed by centrifugation at 12,000 g for 10 min at 4°C. Supernatants were isolated and diluted 1:1 (v/v) with 10 mMol/L ammonium acetate for analysis by ultra-high performance LC-MS (UHPLC-MS) (¹¹).

UHPLC-MS lipid analysis. Samples were analyzed on a Thermo Vanquish UHPLC system (San Jose, CA, USA) coupled online to a Thermo Q Exactive mass spectrometer (Bremen, Germany). Lipids were resolved over a Waters ACQUITY HSS T3 column (2.1 x 150 mm, 1.8 μ Mol/L) using an aqueous phase (A) of 25% acetonitrile and 5 mM ammonium acetate and a mobile phase (B) of 50% isopropanol, 45% acetonitrile and 5 mMol/L ammonium acetate. Samples were eluted from the column using either the solvent gradient: 0-1 min 25% B and 0.3 mL/min; 1-2 min 25-50% B and 0.3 mL/min, 2-8 min 50-90% B and 0.3 mL/min, 8-10 min 90-99% B and 0.3 mL/min, 10-14 min hold at 99% B and 0.3 mL/min, 14-14.1 min 99-25% B and 0.3 mL/min, 14.1-16.9 min hold at 25% B and 0.4 mL/min, 16.9-17 min hold at 25% B and resume flow of 0.3 mL/min. The mass spectrometer was operated in negative ion mode,

scanning in Full MS mode (2 μ scans) from 150 to 1500 m/z at 70,000 resolution, with 4 kV spray voltage, 45 sheath gas, 15 auxiliary gas. Samples were analyzed in randomized order with a technical mixture injected incrementally to qualify instrument performance. Acquired data was then converted from .raw to .mzXML file format using RawConverter. Metabolites were assigned using Maven (Princeton, NJ, USA) (^{12,13}).

Plasma cytokine and chemokine analysis.

Plasma was diluted 1:2 with sample dilution buffer provided by the manufacturer, and proteins were analyzed using the Quantibody Mouse Cytokine Array 1 (RayBiotech, Peachtree Corners, GA) according to the manufacturer's instructions. The signal was visualized using an Amersham Typhoon fluorescence scanner (GE Healthcare Bio-Sciences, Pittsburgh, PA). Data were analyzed using ImageQuant TL software (General Electric).

Statistical analysis.

All statistical analyses were performed using GraphPad Prism version 7.0c (GraphPad Software, Inc., La Jolla, CA), and data were reported as means \pm SEM. Carotid artery dose responses were assessed using a two-way analysis of variance (ANOVA) with a between factor of group and repeated factor of dose. VEGF-A supplementation cell culture experiments were assessed using a two-way ANOVA with a between factor of group and across conditions (Vehicle and VEGF-A). A Sidak's multiple comparisons *post hoc* test was performed when significant main effect differences were detected. Differences across groups in morphological and artery characteristics, water intake, food intake, NO-mediated dilation, ROS, immunoblots, plasma exposure cell culture experiments, plasma cytokines and plasma metabolomics were analyzed by independent samples *t* tests. The relationship between significantly altered metabolites and total and mitochondrial ROS were assessed using linear regressions. Significance was set to $\alpha = 0.05$.

SUPPLEMENTAL RESULTS.

Supplemental Table 1. Tissue mass for soleus and tibialis anterior muscles, subcutaneous WAT and liver.

	Sham (n = 4)	DOXO (n = 8)	<i>P</i> Value
Soleus (mg)	19.5 ± 3.9	17.8 ± 2.8	0.70
Tibialis anterior (mg)	144.0 ± 11.3	133.4 ± 8.6	0.50
Subcutaneous white adipose tissue (mg)	267.8 ± 25.5	255.6 ± 43.9	0.90
Liver (g)	1.5 ± 0.1	1.4 ± 0.4	0.30

Data are the mean ± SEM.

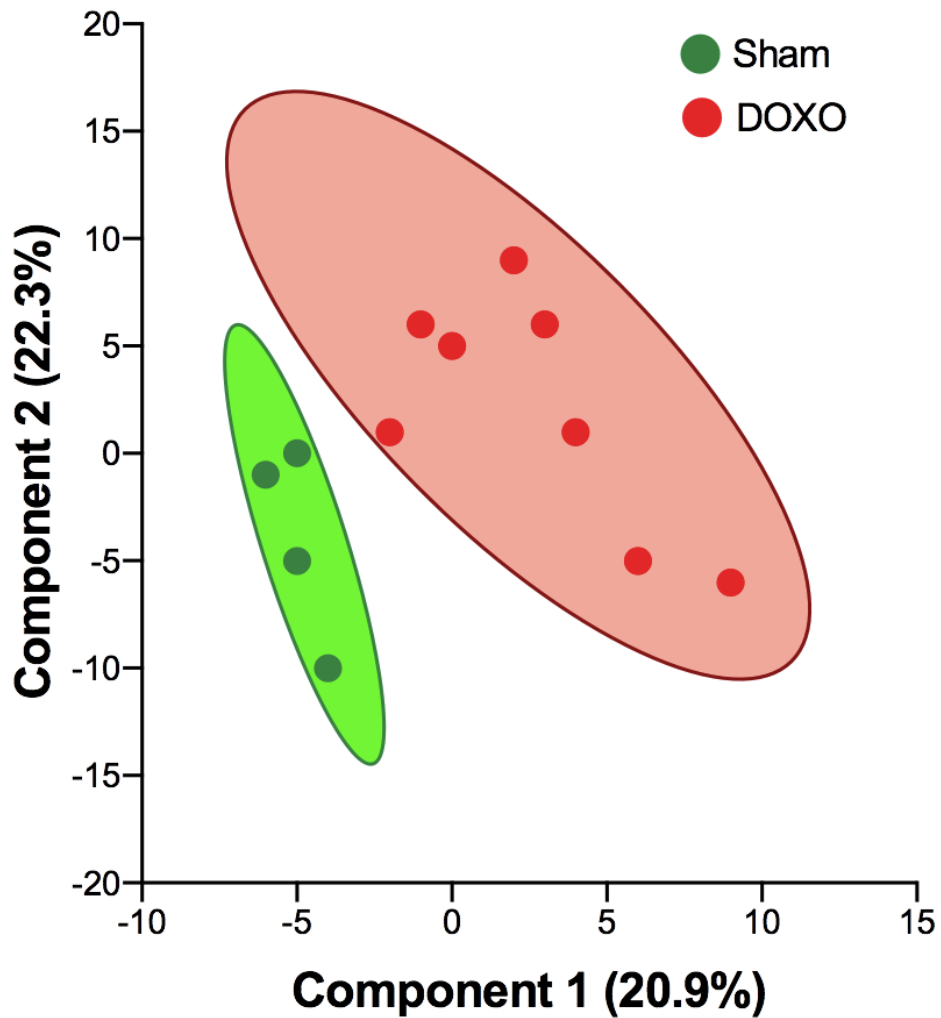
Supplemental Table 2. Individual metabolite abundance in plasma from DOXO and Sham treated mice.

166	N-Acyl-D-glutamate	C06379	Other	3.37E+05	2.49E+05	1.46E+05	5.31E+05	3.18E+05	4.91E+05	1.72E+05	3.07E+05	5.51E+05	3.56E+05	2.70E+05	3.27E+05	3.13E+05	3.41E+05	0.92	4.98E-01
167	Hydroxyacetone phospho	C03505	Other	2.30E+05	2.62E+05	8.14E+04	2.57E+05	1.97E+05	3.47E+05	2.72E+05	2.24E+05	2.80E+05	3.21E+05	2.93E+05	2.71E+05	2.44E+05	2.86E+05	0.85	1.78E-01
168	N-Acetylmethionine	C02712	Other	1.63E+05	9.61E+04	1.76E+05	3.45E+05	1.44E+05	1.50E+05	1.13E+05	4.87E+05	5.02E+05	2.49E+05	3.75E+05	3.43E+05	1.56E+05	3.59E+05	0.44	6.96E-02
169	10-Hydroxydecanoic acid	C02774	Other	3.97E+05	1.46E+06	4.35E+05	8.77E+05	9.09E+05	8.84E+05	7.20E+05	1.79E+06	5.46E+05	7.11E+05	6.49E+05	6.89E+05	8.80E+05	6.69E+05	1.32	2.73E-01
170	2-Oxo-7-methylthioheptan	C17220	Other	1.35E+06	8.76E+05	1.10E+06	1.53E+06	9.20E+05	1.50E+06	7.29E+05	1.73E+06	1.46E+06	1.37E+06	1.88E+06	1.27E+06	1.23E+06	1.41E+06	0.87	2.16E-01
171	L-Homocitrulline	C02427	Other	8.71E+04	6.77E+04	1.37E+05	1.18E+05	8.20E+04	1.04E+05	1.32E+05	1.12E+05	5.30E+04	1.73E+05	5.10E+04	6.66E+04	1.08E+05	5.98E+04	1.81	4.30E-01
172	TMAO (trimethylamine N-oxide)	C01104	Bacterial metabolite	2.13E+06	2.15E+06	8.77E+06	1.78E+06	1.32E+06	2.91E+06	2.16E+06	4.05E+06	3.38E+06	2.76E+06	2.52E+06	2.29E+06	2.15E+06	2.64E+06	0.82	7.43E-01

Supplemental Table 3. Morphological characteristics of mice treated with DOXO with and without oral MitoQ supplementation

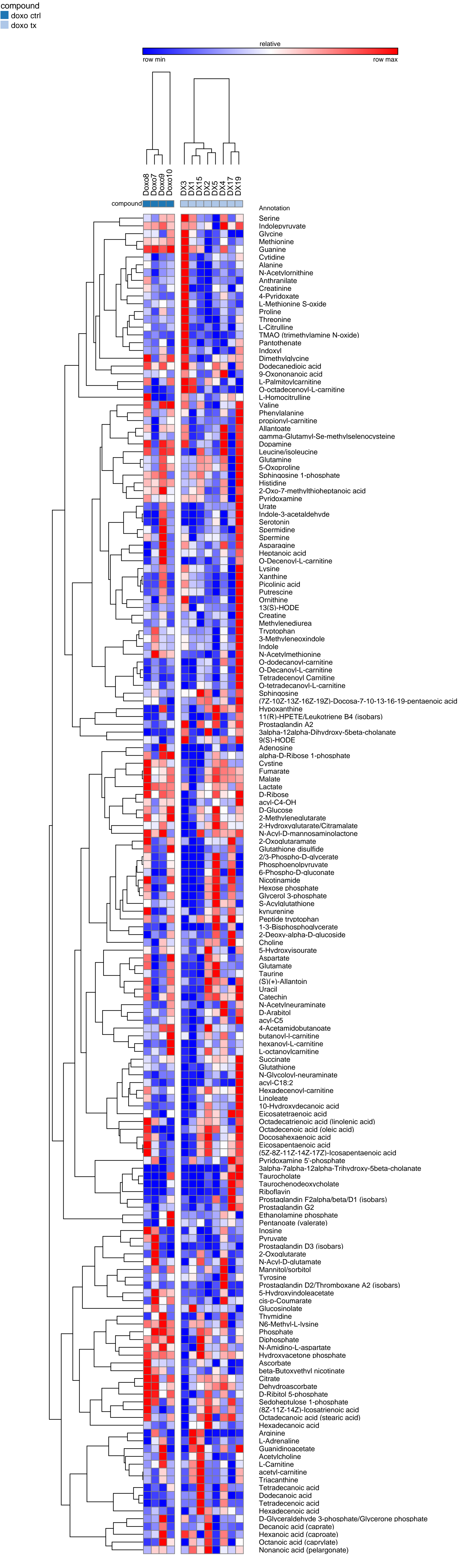
	DOXO (n = 4)	DOXO + MitoQ (n = 5)	<i>P</i> Value
Heart (mg)	120.0 ± 7.1	130.0 ± 7.8	0.355
Quadriceps (mg)	285.2 ± 20.2	300.0 ± 9.1	0.561
Gastrocnemius (mg)	226.8 ± 23.5	235.0 ± 6.5	0.772
Epididymal white adipose tissue (mg)	296.0 ± 32.1	342.5 ± 78.8	0.083

Data are the mean ± standard error of the mean.

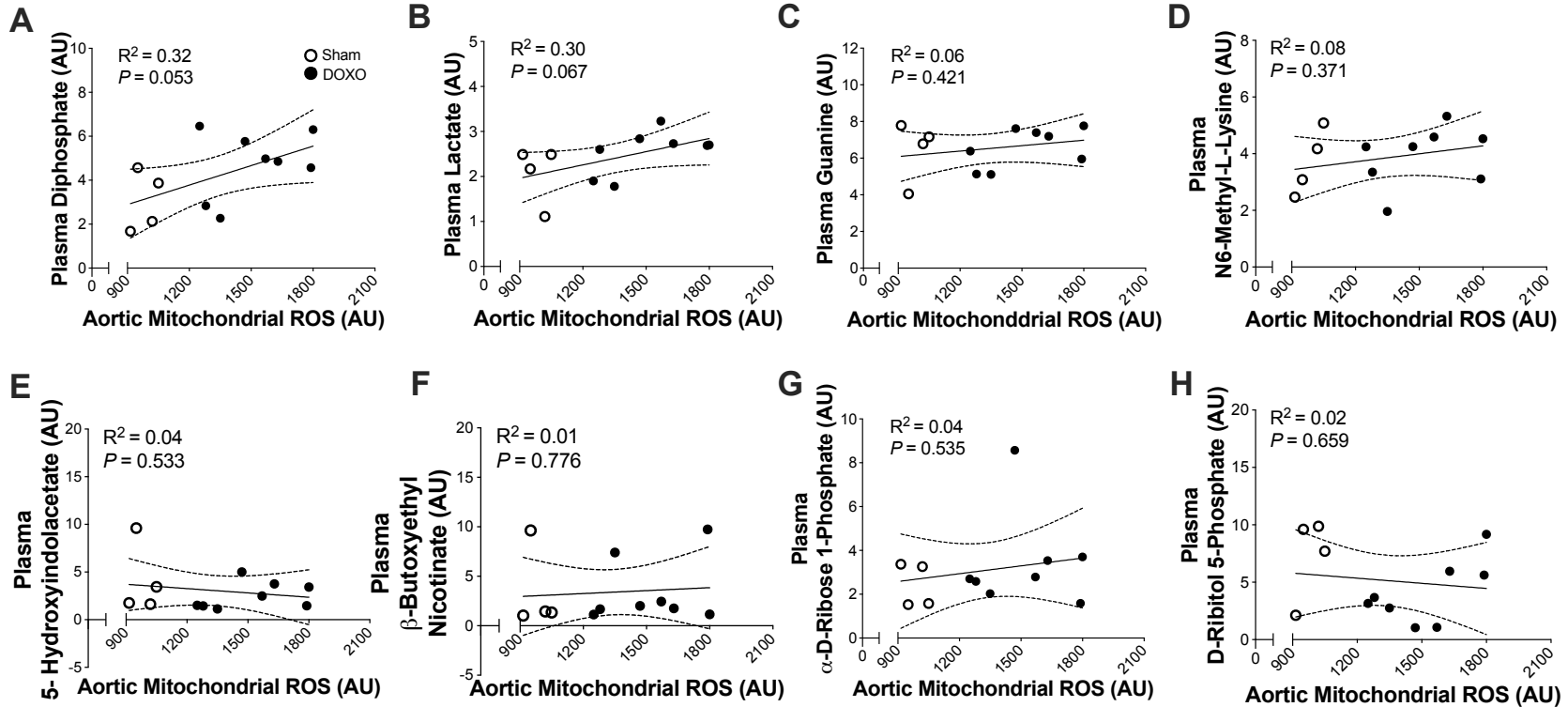


Supplemental Figure S1. Principal components analysis based on partial least squares-discriminant analysis of metabolites in plasma from DOXO and Sham treated mice.

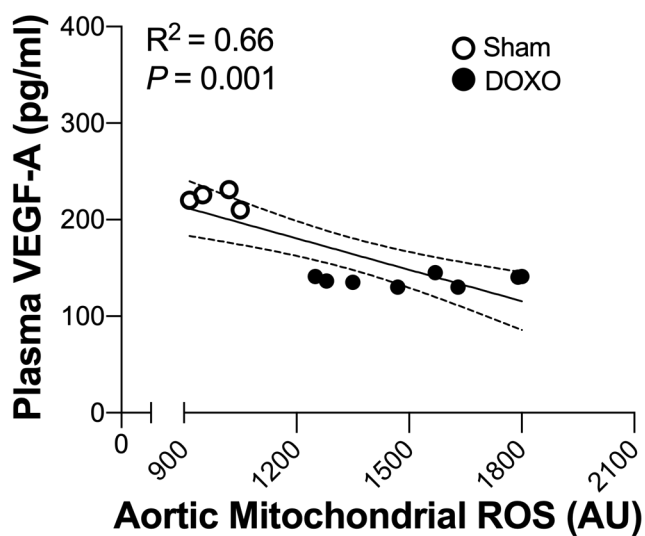
Supplemental Figure S2. Heat map analysis of metabolites in plasma from DOXO and Sham treated mice.



Supplemental Figure 3.



Supplemental Figure S3. Linear regression comparing plasma metabolites significantly altered by doxorubicin (DOXO) and aortic mitochondrial reactive oxygen species (ROS). Linear regression of plasma concentrations of **A)** diphosphate, **B)** lactate, **C)** guanine, **D)** N6-Methyl-L-Lysine, **E)** 5-hydroxyindolacetate, **F)** beta-Butoxyethyl Nicotinate, **G)** alpha-D-Ribose 1 Phosphate, and **H)** D-Ribitol 5-Phosphate (derived from plasma metabolomics analyses), relative to aortic mitochondrial ROS (derived by electron paramagnetic resonance spectroscopy analyses). Dashed lines represent 95% confidence intervals. AU, amplitude units.



Supplemental Figure S4. Linear regression comparing plasma concentration of VEGF-A in Doxorubicin (DOXO) and Sham treated mice with aortic mitochondrial reactive oxygen species (ROS). Linear regression of plasma concentration of VEGF-A (derived from dot blot array analyses) relative to aortic mitochondrial ROS (derived by electron paramagnetic resonance spectroscopy analyses). Dashed lines represent the 95% confidence interval. AU, amplitude units.

REFERENCES

1. Gioscia-Ryan RA, LaRocca TJ, Sindler AL, Zigler MC, Murphy MP, Seals DR. Mitochondria-targeted antioxidant (MitoQ) ameliorates age-related arterial endothelial dysfunction in mice. *J Physiol*. 2014;592(12):2549-2561.
2. Brunt VE, Gioscia-Ryan RA, Richey JJ, et al. Suppression of the gut microbiome ameliorates age-related arterial dysfunction and oxidative stress in mice. *J Physiol*. 2019.
3. Ballak DB, Brunt VE, Sapinsley ZJ, et al. Short-term interleukin-37 treatment improves vascular endothelial function, endurance exercise capacity, and whole-body glucose metabolism in old mice. *Aging Cell*. 2019:e13074.
4. Lesniewski LA, Connell ML, Durrant JR, et al. B6D2F1 Mice are a suitable model of oxidative stress-mediated impaired endothelium-dependent dilation with aging. *J Gerontol A Biol Sci Med Sci*. 2009;64(1):9-20.
5. Durrant JR, Seals DR, Connell ML, et al. Voluntary wheel running restores endothelial function in conduit arteries of old mice: direct evidence for reduced oxidative stress, increased superoxide dismutase activity and down-regulation of NADPH oxidase. *J Physiol*. 2009;587(Pt 13):3271-3285.
6. de Picciotto NE, Gano LB, Johnson LC, et al. Nicotinamide mononucleotide supplementation reverses vascular dysfunction and oxidative stress with aging in mice. *Aging Cell*. 2016;15(3):522-530.
7. Gioscia-Ryan RA, Battson ML, Cuevas LM, Zigler MC, Sindler AL, Seals DR. Voluntary aerobic exercise increases arterial resilience and mitochondrial health with aging in mice. *Aging (Albany NY)*. 2016;8(11):2897-2914.
8. Liao H, He H, Chen Y, Zeng F, Huang J, Wu L. Effects of long-term serial cell passaging on cell spreading, migration, and cell-surface ultrastructures of cultured vascular endothelial cells. *Cytotechnology*. 2014;66(2):229-238.
9. Schindelin J, Arganda-Carreras I, Frise E, et al. Fiji: an open-source platform for biological-image analysis. *Nat Methods*. 2012;9(7):676-682.
10. Gehrke S, Rice S, Stefanoni D, et al. Red Blood Cell Metabolic Responses to Torpor and Arousal in the Hibernator Arctic Ground Squirrel. *J Proteome Res*. 2019;18(4):1827-1841.
11. D'Alessandro A, Reisz JA, Zhang Y, et al. Effects of aged stored autologous red blood cells on human plasma metabolome. *Blood Adv*. 2019;3(6):884-896.
12. Nemkov T, Hansen KC, D'Alessandro A. A three-minute method for high-throughput quantitative metabolomics and quantitative tracing experiments of central carbon and nitrogen pathways. *Rapid Commun Mass Spectrom*. 2017;31(8):663-673.
13. Clasquin MF, Melamud E, Rabinowitz JD. LC-MS data processing with MAVEN: a metabolomic analysis and visualization engine. *Curr Protoc Bioinformatics*. 2012;Chapter 14:Unit14.11.